Self-compensation in semiconductors: The Zn vacancy in Ga-doped ZnO

D. C. Look, K. D. Leedy, L. Vines, B. G. Svensson, A. Zubiaga, F. Tuomisto, D. R. Doutt, and L. J. Brillson

Phys. Rev. B **84**, 115202 — Published 12 September 2011

DOI: 10.1103/PhysRevB.84.115202

Self-compensation in semiconductors: the Zn-vacancy in Ga-doped ZnO

D.C. Look

Semiconductor Research Center, Wright State University, Dayton, OH 45435

K.D. Leedy

Sensors Directorate, Air Force Research Laboratory, Wright-Patterson AFB, OH 45433

L. Vines and B.G. Svensson

Department of Physics, University of Oslo, N-0316 Oslo, Norway

A. Zubiaga and F. Tuomisto

Department of Applied Physics, Aalto University, FI-00076 Aalto, Finland

D.R. Doutt and L.J. Brillson

Department of Physics, Ohio State University, Columbus, OH 43210

Self-compensation, the tendency of a crystal to lower its energy by forming point defects to counter the effects of a dopant, is here quantitatively proven. Based on a new theoretical formalism and several different experimental techniques we demonstrate that the addition of 1.4 x 10^{21}-cm^{-3} Ga donors in ZnO causes the lattice to form 1.7 x 10^{20}-cm^{-3} Zn-vacancy acceptors. The calculated V_{Zn} formation energy of 0.2 eV is consistent with predictions from density functional theory. Our formalism is of general validity and can be used to investigate self-compensation in any degenerate semiconductor material.

I. INTRODUCTION

Self-compensation (SC) in semiconductors, the formation of acceptor-type lattice defects to counter donor-type impurity dopants, or vice versa, has been theoretically predicted to occur in wide-bandgap semiconductor materials; however, its existence has seldom ever been proven because of the difficulty in measuring and matching impurity and point-defect concentrations with donor (N_D) and acceptor (N_A) concentrations. In this work we develop a new theoretical formalism to determine N_D and N_A in degenerate semiconductor materials, and then use it to investigate an important transparent-electrode material, Ga-doped ZnO [1-3]. Then, from secondary-ion mass spectroscopy (SIMS) results, we show that $N_D \approx$ [Ga], as expected, and from positron annihilation results that N_A is consistent with [V_{Zn}], where V_{Zn} is the Zn-vacancy. Finally, from further comparison with SIMS measurements and the application of density functional theory (DFT), we show that N_A can be explained only by V_{Zn}, and not any other impurity or point defect. These results conclusively demonstrate SC in highly doped ZnO, and by inference SC is also possible in other transparent-electrode materials. If present, it will impose a limit on the ultimate conductivity that can be attained, at least under conditions of thermodynamic equilibrium. Indeed, for our ZnO sample the room-temperature resistivity is 2.0×10^{-4} Ω-cm, but elimination of the Zn vacancies would improve it to 0.9×10^{-4} Ω-cm, nearly a world's record for ZnO. Finally, as a check on the model, the value of [V_{Zn}] is consistent with that expected from theoretical formation energies.

II. THEORY

Our theoretical formalism is based on finding an analytical expression for mobility $\mu(N_D,N_A,T)$ and then fitting this expression to the experimental mobility $\mu_{expt}(T)$, obtained from Hall-effect measurements. The Hall experiment also measures carrier concentration n, which in degenerate materials immediately yields a second relationship: $n = N_D - N_A$, independent of temperature.

Degeneracy also simplifies the mobility calculations, because (1) no energy averaging is necessary since all scattering occurs at the Fermi energy, E_f; (2) E_f is a simple and well-known function of n; (3) Matthiessen's Rule ($\mu_{tot}^{-1} = \mu_1^{-1} + \mu_2^{-1} + \mu_3^{-1} + ...$) applies exactly [4,5]; and (4) the *major* scattering is due to ionized impurities and the relevant theory (Brooks-Herring, B-H) contains only well-known parameters [4]. In thin films, we must also consider scattering due to boundaries (surfaces and interfaces), and at higher temperatures, we must include phonon scattering. Thus, $\mu_{tot}^{-1} = \mu_{ii}^{-1} + \mu_{ph}^{-1} + \mu_{bdry}^{-1}$, where μ_{tot} is to be fitted to the experimental mobility, μ_{expt}. Another scattering mechanism, that due to charged grain boundaries [6], may also be important if $n \leq 10^{20}$ cm^{-3}; however, that is not the case for our samples, or indeed for most competitive TCO materials. We can transpose the above equation to read: $\mu_{ii}(N_D,N_A)^{-1} = \mu_{expt}^{-1} - \mu_{ph}(n,T)^{-1} - \mu_{bdry}(n,d)^{-1}$ where T is the absolute temperature and d is the sample thickness. Every term on the right-hand side is either measured or easily calculable from parameters in the literature, and thus we obtain a relationship between N_D and N_A. The other relationship is $n = N_D - N_A$.

The degenerate form of the B-H equation is usually written as $\mu_{ii}(n,N_{ii}) = \mu_{ii0}(n)n/Z^2N_{ii}$, where N_{ii} is the concentration of ionized impurities (or defects) of charge Z, and $\mu_{ii0}(n)$ is given by [4,5]

$$\mu_{ii0}(n) = \frac{24\pi^3 {\varepsilon_0}^2 \hbar^3}{e^3 m^{*2}} \frac{1}{\ln(1+y(n)) - \frac{y(n)}{1+y(n)}} \tag{1}$$

where

$$y(n) = \frac{3^{1/3} 4\pi^{8/3} \varepsilon_0 \hbar^2 n^{1/3}}{e^2 m^*} \tag{2}$$

Here, ε_0 is the static dielectric constant and m* is the effective mass. Usually it is assumed that Z = 1, and if so, then $\mu_{ii}(n,N_{ii}) = \mu_{ii0}(n)(1-K)/(1+K)$, where $K = N_A/N_D$ is the compensation ratio, and $\mu_{ii0}(n)$ can be identified as the maximum possible mobility at a given concentration n because it is the value of μ when $N_A = 0$ [4]. However, for this study it will be necessary to relax the condition Z = 1 and also we will need to generalize the B-H equation to allow for multiple types of donors and acceptors. To carry out this generalization we recognize that each group of donors and acceptors will act as independent scattering centers, and thus we can add their respective scattering *rates*, i.e., the inverse mobilities, essentially invoking Matthiessen's Rule again:

$$\mu_{ii}^{-1} = \mu_{ii0}(n)^{-1}\frac{\sum Z_{Dj}^{\ 2}N_{Dj} + \sum Z_{Aj}^{\ 2}N_{Aj}}{n} = \mu_{ii0}(n)^{-1}\frac{\sum Z_{Dj}^{\ 2}N_{Dj} + \sum Z_{Aj}^{\ 2}N_{Aj}}{\sum Z_{Dj}N_{Dj} - \sum Z_{Aj}N_{Aj}} \qquad (3)$$

In our sample, we will show that there is one main donor, Ga, with $Z_D = 1$, and one main acceptor, the isolated Zn vacancy V_{Zn}, with $Z_A = 2$ (in n-type material) [7,8]. In this case, Eq. 3 becomes $\mu_{ii}(N_D,N_A) = \mu_{ii0}(n)(N_D - 2N_A)/(N_D + 4N_A)$.

For high-temperature analysis, we must add scattering due to optical and acoustic phonons. The optical phonons interact mainly through the polar potential, at least in ZnO, and the acoustic phonons, through the deformation and piezoelectric potentials [5,9]. To characterize the polar optical scattering we use the Howarth-Sondheimer theory [10,11], which gives a mobility

$$\mu_{po}(T) = \frac{2^{3/2}\pi\hbar^2\left(e^{\frac{T_{po}}{T}} - 1\right)\chi\left(T_{po}/T\right)}{e\left(kT_{po}\right)^{1/2}(m^*)^{3/2}\left(\varepsilon_1^{-1} - \varepsilon_0^{-1}\right)} \qquad (4)$$

where T_{po} is the polar-optical temperature (837 K in ZnO, or 72.1 meV), ε_1 is the high-frequency dielectric constant, and $\chi(T_{po}/T)$ is a numerical function introduced by Howarth and Sondheimer. For ZnO (only) we offer a fairly good approximation for $\chi(T_{po}/T)$ over the limited range $T_{po}/T \geq 2.8$, or T ≈ 0 – 300 K: $\chi(T_{po}/T) = [1 + \exp(-0.6T_{po}/T)]^{-1}$. The acoustic phonons, interacting through the deformation potential, lead to a mobility [5,9]:

$$\mu_{ac}(n,T) = \frac{\pi\hbar^4 c_l}{2^{1/2}(m^*)^{5/2}E_1^{\,2}ekT}E_f(n)^{-1/2} \tag{5}$$

where E_1 is the acoustic deformation potential, c_l the longitudinal elastic constant, and $E_f(n)$ the Fermi energy, given by the well-known formula $E_f(n) = (\hbar^2/2m^*)(3\pi^2 n)^{2/3}$ [5]. Lastly, for acoustic phonons interacting through the piezoelectric potential, the associated mobility is [5,9]:

$$\mu_{pe}(n,T) = \frac{2^{3/2}\pi\hbar^2\varepsilon_0}{(m^*)^{3/2}P_{pe}^{\,2}ekT}E_f(n)^{1/2} \tag{6}$$

where P_{pe} is the unitless piezoelectric constant. The three phonon scattering mechanisms are again combined via Matthiessen's Rule: $\mu_{ph}(n,T)^{-1} = \mu_{po}(T)^{-1} + \mu_{ac}(n,T)^{-1} + \mu_{pe}(n,T)^{-1}$.

Finally, in thin films we can have scattering at the boundaries, the surface and interface. Here, we offer a simple, heuristic model that seems to work well for thicknesses d above, say, 20 nm. Under the logical assumption that the boundary-scattering-limited mean free path (mfp) should increase as d increases, we postulate that mfp = d/C, where C is a constant that depends on the

particular system being studied [4,12]. The relevant velocity for scattering should be the Fermi velocity, so the mobility becomes:

$$\mu_{bdry}(d,n,C) = \frac{e}{m^*}\frac{d/C}{v_{Fermi}(n)} = \frac{e}{\hbar}\frac{d/C}{\left(3\pi^2 n\right)^{1/3}} \tag{7}$$

The value of C can be determined by growing multiple samples with various values of d and fitting μ_{expt} vs d to Eq. 8, below. For example, ZnO layers grown on SiO_2 by pulsed laser deposition (PLD) in O_2 at 400 °C and annealed in forming gas (5% H_2 in Ar) at 400 °C were well fitted with C = 4 [4], and PLD ZnO layers grown on Al_2O_3 in Ar at 200 °C required C = 2.5 [12]. Fortunately, however, an accurate value of C is not a requirement for obtaining good values of N_D and N_A for our sample of thickness d = 278 nm. This can be seen immediately by inserting the measured values C = 2.5 and n = 1.1 x 10^{21} cm^{-3} into Eq. 7 to get μ_{bdry} = 527 cm^2/V-s. Since $\mu_{expt} \leq 50$ cm^2/V-s for all samples in this study, boundary scattering is not a major component of the mobility; however, we will still include it for maximum accuracy.

We now combine Eq. 3 with our earlier equation, $\mu_{ii}(N_D,N_A)^{-1} = \mu_{expt}^{-1} - \mu_{ph}(n,T)^{-1} - \mu_{bdry}(n,d)^{-1}$, to get:

$$\mu_{ii}(N_D,N_A)^{-1} = \mu_{ii0}(n)^{-1}\frac{Z_D{}^2 N_D + Z_A{}^2 N_A}{Z_D N_D - Z_A N_A} = \mu_{expt}(T)^{-1} - \mu_{ph}(n,T)^{-1} - \mu_{bdry}(d,n,C)^{-1} \tag{8}$$

where the only unknowns are N_D and N_A. Finally, we solve Eq. 8 simultaneously with $n = Z_D N_D - Z_A N_A$:

$$N_D = \frac{n}{Z_D(Z_D+Z_A)}\left\{\frac{\mu_{ii0}(n)}{\mu_{expt}(T)}[1-Corr(d,n,C,T)] + Z_A\right\} \tag{9}$$

$$N_A = \frac{n}{Z_A(Z_D + Z_A)}\left\{\frac{\mu_{ii0}(n)}{\mu_{expt}(T)}[1 - Corr(d,n,C,T)] - Z_D\right\} \quad (10)$$

where

$$Corr(d,n,C,T) = \frac{\mu_{expt}(T)}{\mu_{ph}(n,T)} + \frac{\mu_{expt}(T)}{\mu_{bdry}(d,n,C)} \quad (11)$$

Here, Corr(d,n,C,T) may be thought of as a correction term (normally small) due to phonon scattering at high temperatures and boundary scattering at small thicknesses. For our unannealed sample, at T = 20 K, Corr = 0.001+ 0.062 = 0.063, and at 300 K, Corr = 0.131 + 0.054 = 0.185. Thus, it is always best, if possible, to measure μ_{expt} at as low a T as possible, say, T < 100 K, to avoid the phonon terms altogether. In this regard, measurements at liquid-nitrogen temperature (77K), if available, should be quite sufficient in most cases. Also, thicker samples are better for avoiding the boundary scattering correction. However, if thick samples and low-temperature measurements are not possible, then Eqs. 9 - 10 can be applied with only slightly reduced accuracy.

III. EXPERIMENT

Eight, 1-cm x 1-cm pieces were cut from a 278-nm-thick ZnO film grown on a 3-inch Al_2O_3 substrate by PLD at 200 °C in an atmosphere of pure Ar. We have earlier showed that the unusual process of PLD growth in pure Ar, without any O_2 in the growth ambient, produces highly conductive ZnO [12]. For the present samples, the as-grown, room-temperature (RT) resistivity was 1.96 x 10^{-4} Ω-cm, without any additional processing, such as annealing. However, to test whether even lower resistivities could be obtained by further processing, we subjected seven of the pieces to rapid thermal annealing in forming gas (5% H_2 in Ar) for 10 min at various temperatures from T_A = 300 – 600 °C. The minimum resistivity obtained was 1.46 x 10^{-4} Ω-cm, at T_A = 500 °C. Although these annealing results are of interest for practical applications, we wish to emphasize that the main

conclusion of this paper, the existence of self-compensation in the form of Zn vacancies, depends only on analysis of the unannealed sample.

Hall-effect measurements were carried out over the range 20 – 300 K. The mobilities for the unannealed sample and those annealed at 450, 500, and 600 °C are shown in Fig. 1. The fits to the curves, using Eq. 8, are also shown, as solid lines. In the fittings, the following parameters in Eqs. 1 - 6 were taken from the literature: $\varepsilon_0 = 8.12\varepsilon_{vac}$, $\varepsilon_1 = 3.72\varepsilon_{vac}$, $T_{po} = 837$ K, $E_1 = 3.8$ eV, $P_{pe} = 0.21$ [9], and $c_l = 1.4 \times 10^{11}$ N/m^2[13]. For the remaining two parameters, the constant C = 2.5 in Eq. 7 was determined from a μ vs d analysis, discussed in Ref. [12], and an effective mass $m^* = 0.34m_0$ produced the best fit of μ vs T for the unannealed sample, as demonstrated by the solid line in Fig. 1. (The upper and lower dashed lines are calculated using different values of m*, $0.30m_0$ and $0.40m_0$, respectively.) Note that our best-fit m* of $0.34m_0$ is larger than the literature value $0.318m_0$ [9] or the value $0.30m_0$ that we and others have typically used for nondegenerate samples [14]. However, it is expected that the conduction band (CB) may be somewhat nonparabolic at the Fermi energy (E_f = 1.3 eV at $n = 1.1 \times 10^{21}$ cm^{-3}), and so our higher value of m* may be taken as a measure of the CB nonparabolicity at E_f. Using $m^* = 0.34m_0$ along with the other parameters mentioned above, we fit Eq. 8 to the mobility data for the unannealed sample and those annealed at 450, 500, and 600 °C. The values of N_D and N_A producing the best fits are displayed in Fig. 1. For the unannealed sample, $N_D = 1.45 \times 10^{21}$ and $N_A = 1.71 \times 10^{20}$ cm^{-3}, where we have assumed that $Z_D = 1$ and $Z_A = 2$. Below we will compare with SIMS to show that N_D consists mainly of the dopant Ga, with slight contributions from H and Al, but that N_A cannot be due to any impurity.

To quantitatively assess the possible impurity involvement in N_D and N_A, secondary-ion mass spectrometry (SIMS) measurements were performed. Calibrations of individual impurities were accomplished with ion-implanted standards. For maximum calibration accuracy, the peak

concentration of a given impurity in the implanted standard was designed to be about the same as the expected concentration of that same impurity in the sample itself. A mass scan of all elements was carried out to determine which were of a sufficient concentration to contribute significantly to the > 10^{21} cm^{-3} donors and the > 10^{20} cm^{-3} acceptors, and thus only impurities of concentration > 10^{18} cm^{-3} were considered further in the analysis. Three impurities, all normally donors, satisfied this criterion: Ga (~ 1.4 x 10^{21} cm^{-3}), H (~ 1 - 9 x 10^{19} cm^{-3}, depending on depth and anneal conditions), and Al (~ 3 x 10^{18} cm^{-3}). Thus, as expected, the donors are dominated by Ga, but H and Al are also included in the total SIMS-derived donor concentration, i.e., SIMS-N_D = [Ga] + [H] + [Al]. The SIMS-N_D's are plotted in Fig. 2 for the unannealed sample and those annealed at 500 and 600 °C, and they are compared with the Hall-N_D's calculated from the respective mobilities at 20 K. In the unannealed sample, the excellent agreement between the Hall and SIMS N_D's, along with the good fit to the overall temperature dependence demonstrated in Fig. 1, shows that the scattering model is basically sound and should also be applicable to the annealed samples. Consider the sample annealed at 600 °C: here the SIMS-N_D has dropped about 10%, with the drop split about evenly between decreases in [H], expected to leave the sample at 600 °C [15], and [Ga]. However, the Hall-N_D has decreased much more, about 45%. Since [Ga] itself drops by only about 5%, the large decrease in N_D has to come from the loss of donor character in some of the Ga atoms, and this can possibly occur through reactions at 600 °C that produce neutral forms of Ga, such as Ga_2O_3 or $ZnGa_2O_4$ [16]. Confirmation of such possibilities will have to await further investigation.

IV. DISCUSSION

We now turn to the identity of the acceptors, of concentration N_A = 1.71 x 10^{20} cm^{-3}. No impurities, except possibly Ga itself, can account for a concentration this high. If Ga were involved, then the associated acceptor would likely be $Ga_{Zn}V_{Zn}$, a singly-charged complex. In that case, we

would have $Z_A = 1$ and Eqs. 9 and 10 would give $N_D = 1.64 \times 10^{21}$ and $N_A = 5.40 \times 10^{20}$ cm^{-3}. For Ga to account for all the acceptors, and all of the donors except H and Al, we would need $[Ga] = N_D - [H] - [Al] + N_A \approx 2.0 \times 10^{21}$ cm^{-3}, and that is outside the error of our SIMS value, $[Ga] \leq 1.4 \times 10^{21}$ cm^{-3}. Thus, we conclude that the dominant acceptor must be a doubly-charged point defect, at a concentration of about 1.7×10^{20} cm^{-3}. The potential acceptor-like point defects are the Zn vacancy, V_{Zn}, the O interstitial, O_I, and the O antisite, O_{Zn}. To get an estimate on which of these defects is most likely we can assume quasi-equilibrium growth conditions and compare the formation energies E_F's calculated from density functional theory DFT [7,8]. It turns out that for n-type material, under either Zn-rich or O-rich growth conditions, the E_F's for both O_I and O_{Zn} are at least 2 eV higher than that of V_{Zn}. The concentration of a particular species can be approximated by $C \approx N_{sites}\exp(-E_F/kT_G)$, where N_{sites} is the density of sites available for that species and $T_G = 473$ K is the growth temperature. For V_{Zn}, $N_{sites} \approx 4 \times 10^{22}$ cm^{-3}, and $C = N_A = 1.7 \times 10^{20}$ cm^{-3}, so that the predicted $E_F(V_{Zn}) \approx 0.22$ eV. Theoretical values for $E_F(V_{Zn})$ have been calculated by DFT, but these values depend on the choices of exchange and correlation functionals. In Ref. 7, localized functionals (GGA approximation, in this reference) are used and $E_F(V_{Zn}^{2-})$, for a Fermi energy E_{Fermi} at the CB minimum (E_{CBmin}), ranges between + 1.8 eV for Zn-rich growth to -1.9 eV for O-rich growth. In Ref. 8, several local and nonlocal combinations of functionals are compared, and a screened exchange (sX) functional, which produces an accurate bandgap $E_g = E_{CBmin} - E_{VBmax} = 3.41$ eV, gives $E_F(V_{Zn}^{2-}) = +4.1$ eV for Zn-rich growth and + 0.2 eV for O-rich growth. However, E_{Fermi} in our samples will in general be different from 3.41 eV, because the extremely high concentration ($\sim 10^{21}$ cm^{-3}) of Ga atoms will affect it in several ways: (1) the CB will be shifted downward because of exchange and correlation effects arising from the donor electrons (bandgap narrowing or renormalization) [17,18]; (2) the host CB states will hybridize with the Ga donor states and induce nonparabolicity [18]; and

(3) the donor electrons will fill states well into the CB and thus effectively increase the bandgap (Moss-Burstein effect) [17,18,19]. For comparison with the *nondegenerate* DFT case, the new equilibrium bandgap will be $E_{DFT}(n) = E_{CB}(k_{Fermi}) - E_{VBmax}$. To determine $E_{DFT}(n)$, some relevant information can be obtained from a simple optical absorption (OA) threshold measurement, which gives $E_{OptAbs} = 3.85$ eV for a sample with $n = 1 \times 10^{21}$ cm^{-3}, grown on double-side polished Al_2O_3 (in order to carry out absorption measurements). The OA experiment was performed with the light direction parallel to the c-axis which means the light is polarized perpendicular to the c-axis. For such a polarization, transitions are allowed from either of the top two, nearly degenerate, valence bands (Γ_7 and Γ_9 symmetry) to the lowest conduction band (Γ_7) at k = 0 [20]. Since the absorption transition is vertical in k-space, we can write $E_{OptAbs} = E_{CB}(k_{Fermi}) - E_{VB}(k_{Fermi}) = E_{DFT}(n) + E_{VBmax} - E_{VB}(k_{Fermi})$. Thus, $E_{DFT}(n) = E_{OptAbs} - (\hbar^2/2)[(k_x^2 + k_y^2)/ m_{hh\perp}^* + k_z^2/ m_{hh//}^*]$, where $m_{hh\perp}^*$, and $m_{hh//}^*$ are the effective masses of the heavy holes, perpendicular and parallel to the c axis, respectively, and $k_{Fermi} = (3\pi^2 n)^{1/3}$. Also, $k_x^2 + k_y^2 + k_z^2 = k^2 = k_{Fermi}^2 = (3\pi^2 n)^{2/3}$. Unfortunately, $m_{hh\perp}^*$ and $m_{hh//}^*$ are not well-known quantities, but some recently reported values are $m_{hh\perp}^* = 0.8m_0$ and $m_{hh//}^* = 5.0m_0$ [21]. The optical-absorption threshold will occur at the highest point in the VB consistent with $k = k_{Fermi}$, and for $n = 10^{21}$ cm^{-3}, that point is $k_x = k_y = 0$, and $k_z = k_{Fermi} = 3.1 \times 10^9$ m^{-1}, giving $E_{DFT}(n) = 3.85 - 0.073 = 3.78$ eV. Interestingly, the new value of $E_{CBmin} - E_{VBmax}$ is then $3.78 - \hbar^2k^2/2m_e^* = 3.78 - 1.07\text{eV} = 2.71$ eV which may be taken as the renormalized bandgap. Our $E_F(V_{Zn}^{2-})$ values for the sX functional must therefore be corrected by -2(3.78 - 3.41) = -0.74 eV and thus we get $E_F(V_{Zn}^{2-}) = + 4.1 - 0.7 = 3.4$ eV for Zn-rich growth and $+0.2 - 0.7 = -0.5$ eV for O-rich growth, respectively . For comparison, another DFT approach (LDA + U) [7], gives $E_F(V_{Zn}^{2-}) = + 1.8$ eV for Zn-rich growth, and – 1.9 eV for O-rich growth, before corrections for E_{Fermi}, and thus 1.1 eV and -2.6 eV, respectively, after corrections. Clearly, our Hall-effect-derived value of + 0.2 eV is within the

theoretical ranges presented in both of these works, and thus our hypothesis, that the dominant acceptor is V_{Zn}, is consistent with the predictions of DFT.

Finally, we consider the question of *direct* evidence for large quantities of V_{Zn} in our samples. For this we apply positron annihilation spectroscopy (PAS), a technique that is very sensitive to negatively-charged vacancies such as V_{Zn} in ZnO [22,23]. To get good signal strength, we used two thicker PLD samples, one Ga-doped, and the other undoped. The PAS-determined concentrations of isolated Zn vacancies [V_{Zn}] were $\geq 10^{19}$ cm^{-3} for the Ga-doped sample, and $\leq 10^{18}$ cm^{-3} for the undoped sample. (The lower limit on [V_{Zn}] for the doped sample is due to saturation of the PAS signal at [V_{Zn}] $\approx 10^{19}$ cm^{-3}.) Two conclusions are evident: (1) [V_{Zn}] is *at least* 10^{19} cm^{-3} and thus must be the dominant acceptor since it is far larger than any *impurity* of acceptor-type character; and (2) [V_{Zn}] of the undoped sample is more than an order of magnitude below that of the Ga-doped sample, showing that the heavy donor incorporation produces large quantities of compensating point-defect acceptors. (It should also be noted that a signal sometimes seen for vacancy clusters [23,24] was at least two orders of magnitude smaller than that for *isolated* vacancies, showing that only the latter are important.)

Optical evidence for [V_{Zn}] is also found. Depth-resolved cathodoluminescence (DRCL) measurements have shown that bands in the 1.7 – 2.1 eV region correlate well with V_{Zn} concentrations [24]. Indeed, these bands are not strong in most as-grown, nondegenerate ZnO samples, which instead are dominated in the deep region by a green band at 2.4 – 2.5 eV [25]. However, high-energy electron irradiation in such nondegenerate samples produces EPR lines known to be due to V_{Zn} and also a strong photoluminescence band at 1.8 eV, attributed to shallow-donor-V_{Zn} pair (DAP) recombination [25]. Our present, unannealed, Ga-doped sample also has a dominant peak near 1.8 eV, as shown in Fig. 3. in agreement with the presence of V_{Zn}. Here we

compare the samples annealed at 300 °C and 550 °C, because neither of these samples had been subjected to post-anneal processing. Our Hall-effect analysis gives $N_D = 1.44 \times 10^{21}$ and $N_A = 1.64 \times 10^{20}$ cm^{-3} for the 300 °C sample (very close to N_D and N_A of the unannealed sample), and $N_D = 9.25 \times 10^{20}$ and $N_A = 0.33 \times 10^{20}$ cm^{-3} for the 550-°C sample. In Fig. 3, the dashed curve is the 300-°C sample intensity normalized to that of the 550-°C sample in the near-band-edge region (~ 3.5 eV), in order to visually compare the relative intensities of the peaks near 1.8 eV. Qualitatively, the 300-°C sample has a larger 1.8-eV peak, in agreement with the larger N_A found from the Hall-effect analysis. More quantitatively, we might associate the ratio $R_{CL} = I(1.8\text{ eV})/I(3.5\text{ eV})$ with$R_{Hall} = N_A/N_D$, and thus compare $R_{CL}(300)/R_{CL}(550) = 2.5$, and $R_{Hall}(300)/R_{Hall}(550) = 3.4$, which should be considered to be satisfactory agreement considering the many unknown factors affecting the optical line intensities. Thus, the DRCL measurements give further evidence that heavy donor doping induces V_{Zn} acceptors.

Although our experimental work in this investigation has concentrated on the Zn vacancy in ZnO, the mobility model presented here is applicable to all degenerate semiconductors for which values of m*, ε_0, ε_1, T_{po}, E_1, P_{pe}, and c_l are available. (Note that Ref. [9] lists such values for 19 materials.) In particular, the formulas for N_D and N_A (Eqs. 9 and 10) can be immediately applied to other ZnO results already present in the literature. As an example, consider the ZnO sample with one of the lowest ever reported resistivities, $\rho = 8.12 \times 10^{-5}$ Ω-cm [26]. It was grown by PLD on quartz at 300 °C to a thickness of 200-nm, and Hall-effect measurements gave $\mu = 30.96$ cm^2/V-s, and $n = 1.46 \times 10^{22}$ cm^{-3}, at room temperature. From these values of μ and n, we can use Eqs. 9 and 10 to calculate $N_D = 1.76 \times 10^{21}$ and $N_A = 1.50 \times 10^{20}$ cm^{-3}, under the assumption that $m^* = 0.34m_0$ and C = 2.5. Then, assuming that $N_A = [V_{Zn}]$, as with our sample, we get $E_F(V_{Zn}) \approx 0.27$ eV, very close to

our value of 0.22 eV. The higher $N_D = 1.76 \times 10^{21}$ cm^{-3}, compared with our value of 1.45×10^{21} cm^{-3}, may be due to the higher Ga content in their target, 5% vs our 3%. In any case, the close overall agreement between these two studies, especially the very high concentrations of acceptors of near equal magnitudes, is totally consistent with the idea of point-defect compensation in heavily-doped semiconductors.

V. SUMMARY

In summary, we have quantitatively demonstrated self-compensation in a highly doped, wide-bandgap semiconductor, ZnO. To accomplish this task, we have developed a theoretical formalism to calculate donor and acceptor concentrations from mobility measurements in degenerate semiconductors and have applied it to Ga-doped ZnO. In conjunction with Hall-effect, SIMS, and PAS measurements, we have shown that N_D is comprised mostly of Ga, with small contributions from H and Al, and that N_A is due to Zn vacancies. The Zn-vacancy concentration is consistent with that predicted by density-functional theory for nearly stoichiometric growth conditions.

ACKNOWLEDGMENTS

We wish to thank T.A. Cooper for the Hall-effect measurements and B. Claflin for helpful discussions. Support was provided by the Sensors Directorate of the Air Force Research Laboratory, AFOSR Grant FA9550-10-1-0079, NSF Grant DMR0803276, the Norwegian Research Council (Nanomat program), and the Academy of Finland.

References

1. S.J. Pearton, D.P. Norton, K. Ip, Y.W. Heo, and T. Steiner, Prog. In Mater. Sci. 50, 293 (2005).
2. Minami, T, Semicond. Sci. Technol. 20, S35 (2005).
3. H. Liu, V. Avrutin, N. Izyumskaya, Ü. Özgür, and H. Morkoç, Superlattices and Microstructures **48**, 458 (2010).
4. D. C. Look, K. D. Leedy, D. H. Tomich, and B. Bayraktaroglu, Appl. Phys. Lett. **96**, 062102 (2010).
5. D.C. Look, *Electrical Characterization of GaAs Materials and Devices* (Wiley, New York, 1989).
6. K. Ellmer and G. Vollweiler, Thin Solid Films **496**, 104 (2006).
7. A. Janotti and C.G. Van de Walle, Phys. Rev. B **76**, 165202 (2007).
8. S.J. Clark, J. Robertson, S. Lany, and A. Zunger, Phys. Rev. B **81**, 115311 (2010).
9. D.L. Rode, Semiconductors and Semimetals **10**, 1 (1975).
10. D.J. Howarth and E.H. Sondheimer, Proc. Roy. Soc. A **219**, 53 (1953).
11. E.H. Putley, *The Hall Effect and Semiconductor Physics* (Dover, New York, 1960).
12. R.C. Scott, K.D. Leedy, B. Bayraktaroglu, D.C. Look, and Y-H. Zhang, Appl. Phys. Lett. **97**, 072113 (2010).
13. P. Gopal and N.A. Spaldin, J. Electronic Mater. **35**, 538 (2006).
14. D.C. Look, J. Appl. Phys. 104, 063718 (2008).
15. N. Nickel, Phys. Rev. B **73**, 195204 (2006).
16. T-Y. Park, Y-S. Choi, J-W. Kang, J-H. Jeong, S-J. Park, D-M. Jeon, J-W. Kim, and Y-C. Kim, Appl. Phys. Lett. **96**, 051124 (2010).

17. B.E. Sernelius, K.-F. Berggren, Z.-C. Jin, I. Hamberg, and C.G. Granqvist, Phys. Rev. B. 37, 10244 (1988).

18. A. Walsh, J.L.F. Da Silva, and S-H. Wei, Phys. Rev. B **78**, 075211 (2008).

19. N.C. Giles, C. Xu, M.J. Callahan, B. Wang, J.S. Neal, and L.A. Boatner, Appl. Phys. Lett. 89, 251906 (2006).1

20. G. Dresselhaus, Phys. Rev. B **105**, 135 (1957).

21. S.L. Shi and S.J. Xu, J. Appl. Phys. **109**, 053510 (2011).

22. F. Tuomisto, V. Ranki, K. Saarinen, and D.C. Look, Phys. Rev. Lett. **91**, 205502 (2003).

23. A. Zubiaga, F. Tuomisto, V. A. Coleman, H. H. Tan, C. Jagadish, K. Koike, S. Sasa, M. Inoue, and M. Yano, Phys. Rev. B **78**, 035125 (2008).

24. Y-F. Dong, F. Tuomisto, B.G. Svensson, A. Yu. Kuznetsov, and L.J. Brillson, Phys. Rev. B **81**, 081201(R) (2010).

25. L.A. Kappers, O.R. Gilliam, S.M. Evans, L.E. Halliburton, and N.C. Giles, Nucl. Instr. and Meth. in Phys. Res. B **266**, 2953 (2008).

26. S-M. Park, T. Ikegami, and K. Ebihara, Thin Solid Films **513**, 90 (2006).

Figure Captions

Figure 1. Experimental (points) and theoretical (solid and dashed lines) mobilities for Ga-doped ZnO samples grown at 200 °C in pure Ar and annealed at various temperatures in forming gas.

Figure 2. A comparison of donor concentrations determined by Hall mobility analysis (solid lines), and SIMS measurements of [Ga] + [H] + [Al] (dashed lines).

Figure 3. Cathodoluminescence spectra for Ga-doped ZnO samples grown at 200 °C in pure Ar and annealed at 300 °C and 550 °C, respectively, in forming gas. The dashed curve represents the 300-°C sample intensity normalized to that of the 550-°C sample in the near-band-edge region (3.5 eV) in order to compare the relative intensities of the peaks near 1.8 eV.

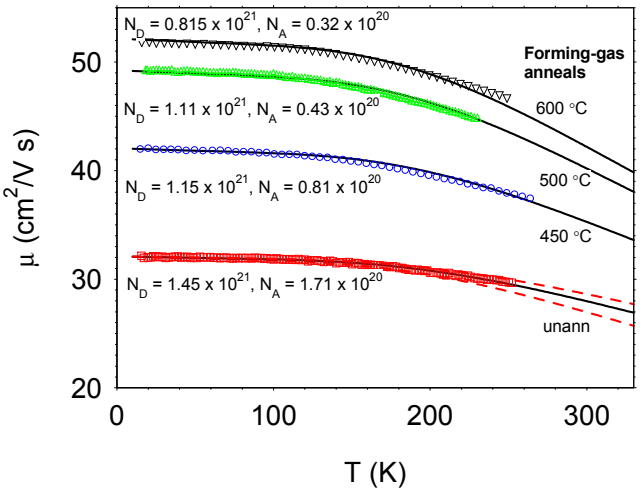

Figure 1. Experimental (points) and theoretical (solid and dashed lines) mobilities for Ga-doped ZnO samples grown at 200 °C in pure Ar and annealed at various temperatures in forming gas.

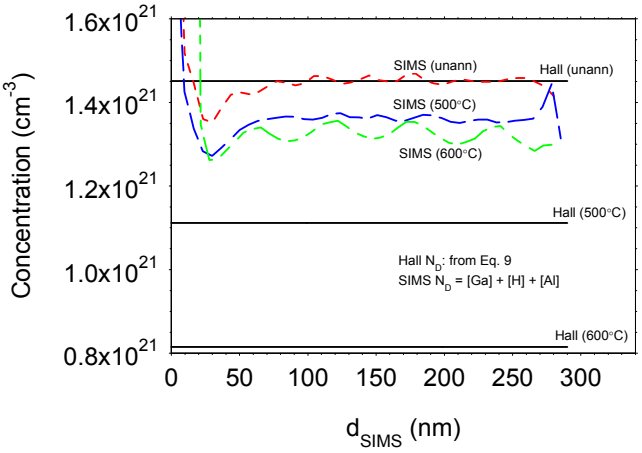

Figure 2. A comparison of donor concentrations determined by Hall mobility analysis (solid lines), and SIMS measurements of [Ga] + [H] + [Al] (dashed lines).

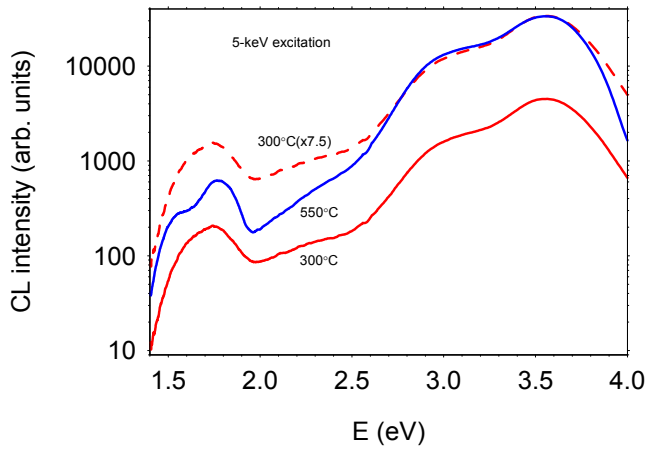

Figure 3. Cathodoluminescence spectra for Ga-doped ZnO samples grown at 200 °C in pure Ar and annealed at 300 °C and 550 °C, respectively, in forming gas. The dashed curve is the 300-°C sample intensity normalized to that of the 550-°C samplein order to compare relative intensities of the peaks near 1.8 eV.